Nanoparticle orientation distribution analysis and design for polymeric piezoresistive sensors

AUTHORS
Marianne Fletcher Clayton [a], R. Adam Bilodeau [b], Anton E. Bowden [a], David T. Fullwood [a, c]

AFFILIATIONS
[a] Mechanical Engineering Department, Brigham Young University, Provo, UT 84602, United States
[b] Mechanical Engineering Department, Purdue University, 585 Purdue Mall, West Lafayette, IN 47907, United States
[c] Corresponding author: 350 EB, Mechanical Engineering Department, Brigham Young University, Provo, UT 84602, United States
Email: dfullwood@byu.edu
Phone: +1 801-422-6316

1 ABSTRACT

Piezoresistive sensors, with polymer matrices and conductive nanoparticles, are a relatively new addition to the sensor class, with the potential to transform such fields as wearable sensors and the internet of things. The unusual inverse piezoresistive behavior of the sensors has been modeled using quantum tunneling and percolation theory. However, the impact of the distribution of conductive particles in the matrix, and specifically their relative orientation, has not been well studied. The initial and deformed distribution of orientations greatly influences the sensor behavior, since the quantum tunneling model is highly sensitive to the polymer gaps between nanoparticles; the evolution of these gaps under deformation is strongly dependent upon the relative orientation of neighboring particles, and determines electron transport properties, and overall sensor response. In this paper a simple analytical model for isotropic orientation distribution and subsequent Poisson-based gap evolution is compared with a more sophisticated finite element and random resistor network analysis. The new numerical model was able to explain previously unexplained physical behavior and is used to design sensors with specific desired characteristics. The appropriateness of the previously assumed percolation behavior is also examined via the model and generalized effective medium theory.

Keywords: piezoresistive sensor, percolation theory, finite element analysis (FEA), nanocomposite

2 INTRODUCTION

There is a rapidly increasing demand for wearable sensors in medical and consumer goods. Traditional metal foil sensors do not have adequate flexibility for biomechanical applications. Piezoresistive polymer composites represent an exciting new technology to fill the need for flexible sensors. Rubber-like polymers (PDMS [1-5], natural rubbers [6, 7]) can be made into conductive polymer composites and / or sensors by the addition of a conductive filler (e.g., carbon black [1, 2, 8-10], carbon nanotubes [4, 8, 9, 11-13], graphene [3, 14-16] or metal nanowires [17, 18]). A variety of such sensors were classified and summarized in reviews by Amjadi [19], Fiorillo [20], and Duan [21]. Examples of applications for such sensors include measuring range of motion for joints [12, 16, 22, 23], pulse [17], and breathing [7, 16]. Another

important application for these sensors is sensing improvements for robotic applications [5, 20, 24].

However, the response of these sensors to deformation is significantly more complex than that of metal foil technology, making sensor optimization more difficult, and often reliant upon empirical testing. Since the matrix polymer is fundamentally an insulator, electrical conductivity across such materials depends upon the presence of connected networks of the conductive filler. The electrical resistance between the particles is usually the dominant contributor to the overall material resistivity. If the gaps between neighboring particles are on the order of a few nanometers, electricity can flow via quantum tunneling. This paper will consider only sensors where this phenomenon is present. The evolution of gaps between neighboring particles, and the characteristics of the percolating particle network, control the piezoresistive response. This paper builds upon previous modeling efforts by applying a finite element analysis (FEA) to determine the gap evolution between particles and combining it with a random resistor network to determine macro-scale electrical response. Various insights into the relationships between particle geometrical distribution and sensor response are obtained. The responses considered in this paper are for quasi-static situations and do not include consideration of dynamic response, including viscoelastic and hysteresis effects.

In particular, we have chosen to investigate the response of nanocomposite sensor comprised of a silicone matrix with nickel nanostrand filler particles. Modeling the unusual (negative) piezoresistive behavior of this material presents a challenge [25, 26], with the combined complexity of quantum tunneling behavior between neighboring conductive filler particles and percolative behavior across the sample. Quantum tunneling is described by quantum mechanics and explains how an electron can cross a potential energy barrier that would block electrical flow by classical theories. Each gap between two neighboring nanoparticles (that have presumably been pushed together by the manufacturing process, while being held slightly apart by the long-chain polymer molecules) can be considered as a potential location for quantum tunneling [11, 24, 25, 27-32]. Equation 1 shows the tunneling resistivity across a gap between two nanoparticles, where ρ is tunneling resistivity, h is Planck's constant, e is the charge of an electron, m_e is the mass of an electron, λ is barrier height, and s is the junction gap distance [33].

$$\rho(s) = \frac{h^2}{e^2\sqrt{2m_e\lambda}} \exp\left(\frac{4\pi\sqrt{2m_e\lambda}}{h} s\right) \quad 1$$

Barrier height (λ) is the electrical potential difference between the two nanoparticles and junction gap distance (s) is the distance between the two nanoparticles. Both of these parameters were experimentally measured for polymer matrices using the procedure described by Koecher [26]. Values for junction gap distance used in this work were 0.47 eV for Sylgard 184 and 0.27 eV for Ecoflex, which correspond to two silicone polymer matrix materials which have previously been reported for this type of sensor [25, 26, 34]. Values between 0.2-1 eV are typical of polymers [35].

In addition to exhibiting quantum tunneling behavior, conductive nanocomposites also represent a quintessential percolation-type system because of the large distance in resistivity between the insulative matrix and conductive polymer. The overall electrical resistance through the material is dominated by the presence of connected paths of filler. As the volume fraction of filler increases, a critical volume fraction, ϕ_c, is reached, when connected pathways begin to form and conductivity increases rapidly [36]. Similar changes in resistance happen by changing the size or type of the nanoparticles [37].

For the sensing material of interest to this paper, the volume fraction of filler remains constant, but the distribution of gap distances between particles evolves with strain, thus modifying the conductivity of potential pathways across the sensor. It has been hypothesized that the dramatic change in gap conductivity when the sample is strained is analogous to increasing (or decreasing) the volume fraction of conductive segments in the material, leading to a percolation-type behavior, with a critical strain at which conductivity increases rapidly [38]. One objective of this paper is to determine whether a percolation-based model reflects the actual behavior of the system.

The generalized effective media equation (GEM) [38] is one way to model the percolative behavior. The GEM equation combines effective media (EM) theories with percolation theory to calculate the overall conductivity of a composite with an insulating matrix and conductive filler [39]. Effective media theories combine the electrical properties of each component in the composite as shown in Equation 2 where ϕ is the volume fraction of filler, σ_m is the conductivity of the neat polymer matrix, σ_f is the conductivity of the filler material, σ_b is the conductivity of the bulk material, and n is the dimension.

$$(1-\phi)\frac{(\sigma_m-\sigma_b)}{\sigma_m+(n-1)\sigma_b}+\phi\frac{\left(\sigma_f-\sigma_b\right)}{\sigma_f+(n-1)\sigma_b}=0 \qquad 2$$

The GEM equation includes a threshold, ϕ_c, as well as critical exponents s and t (see Equation 3) that all relate to the idea that in a percolative system there is a dramatic increase in conductivity past a certain percolation threshold. A is a constant related to the percolation threshold (see Equation 4). The GEM equation in this form assumes perfect conductivity between filler particles that touch each other (i.e. no quantum tunneling gaps). The fit of the GEM and EM equations will be compared with the composite system studied here to test the accuracy of using a percolation model.

$$\frac{(1-\phi)\left(\sigma_m^{1/s}-\sigma_b^{1/s}\right)}{\sigma_m^{1/s}+A\sigma_b^{1/s}}+\frac{\phi\left(\sigma_f^{1/t}-\sigma_b^{1/t}\right)}{\sigma_f^{1/t}+A\sigma_b^{1/t}}=0 \qquad 3$$

$$A=\frac{1-\phi_c}{\phi_c} \qquad 4$$

Many conductive nanocomposite models use the GEM equation [40-46]. However, previous research has also highlighted the fact that the resistance across the percolating network is not defined simply by the resistance of the filler particles [47-49]. The actual resistance of the filler is orders of magnitude smaller than the resistance of the nano-scale polymer gaps between particles; i.e. the network resistance is dominated by the quantum tunneling resistance across these tiny gaps. Hence a revised model is required that somehow accounts for the distribution of gaps rather than the volume fraction of filler.

Several models combine percolation theory and quantum tunneling into one model [25, 47, 48, 50, 51]. Johnson, et al. [25] combined quantum tunneling with Equation 3 by assuming that, for a given volume fraction of filler, there is a certain distribution of gaps between filler particles that can be thought of as a lattice of switches between components of the filler network. The number fraction of tunneling junctions in this lattice is given by Q, and a critical number fraction of tunneling junctions (Q_c) is used in the percolation theory, rather than the filler volume fraction (ϕ) and critical volume fraction (ϕ_c). Equation 3 was used to calculate the resistivity of the matrix across the gap (ρ_m) as a function of barrier height.

Another important aspect of a piezoresistive model involves the change of the geometry between two filler particles with strain. The resistance of a particular gap has an exponential relationship with gap size according to Equation 1, so small changes in gap distance have a large impact on the overall resistance. Simplified models of the piezoresistive behavior have been reported – in particular, a framework that simulates evolution of distance between particles using a Poisson contraction assumption, and combines it with a percolation approach [25]. This model assumed a random distribution of particle orientations that remained constant when the material was strained (i.e. the vector connecting the two closest points between a pair of neighboring particles did not change direction under strain). Gaps that aligned with the tensile direction were lengthened, while gaps in a perpendicular direction were shortened according to the Poisson's ratio. This model will be referred to as the Simple Poisson Contraction model (or SPC) in this work.

The SPC model would be approximately correct if the filler particles and matrix had similar elastic modulae, and if only small strains were assumed. However, for many nanocomposite materials (including the specific sensor material under consideration), the filler particles (i.e., nickel particles) are stiffer than the matrix material (silicone) by several orders of magnitude, causing severe realignment of the particles (and affiliated gaps) under large strains. Finite element analysis (FEA) is required in order to better estimate the subsequent gap evolution and resultant conductivity. For example, Kale [52] found that accounting for filler alignment significantly impacted the percolative model. In addition to having a more complete model for evolution of particle gap with strain, another important benefit of more detailed analysis is the potential to design a sensor to behave in a desired way. For example, a study of the relationship between initial particle alignment and resultant sensor behavior could motivate a sensor design with optimized particle orientation in order to achieve a high gauge factor, or a specific characteristic resistance.

This paper assesses the accuracy of the assumptions of the SPC model through comparison with a more sophisticated FEA model; it also evaluates the potentially increased accuracy of a modified SPC model that incorporates the percolative nature of the piezoresistive response of the sensor material (i.e., a percolative SPC model) by applying a random resistor network model to capture the underlying resistive behavior. The resultant percolative SPC model is demonstrated to exhibit the complex physical behavior not represented by the previous simple SPC model

3 METHODS

3.1 Evolution of Particle Gap Distribution from Finite Element Analysis

3.1.1 Basic Geometry

In this work, the nanoparticles are assumed to be cylindrically shaped for the FEA model. As can be seen in Figure 3-1 of the as-manufactured nanostrands, the particles actually have a very branched structure. However, before being used in the nanocomposite sensors this network is broken into small particles, and subsequently pushed through a screen to break the network into even smaller nanoparticles. The branched nature of the nanoparticles may impact the initial range of orientations of the nanoparticles and would certainly affect attempts at physically aligning the nanoparticles in manufacturing; but where the branches cross, the high aspect ratio means that they still behave as two long rods locally. Hence, while the cylindrical assumption does not perfectly describe the overall shape of the nanoparticles, at the local level (in the

vicinity of a given junction between neighbors) the approximation of cylindrical shape is expected to be sufficient.

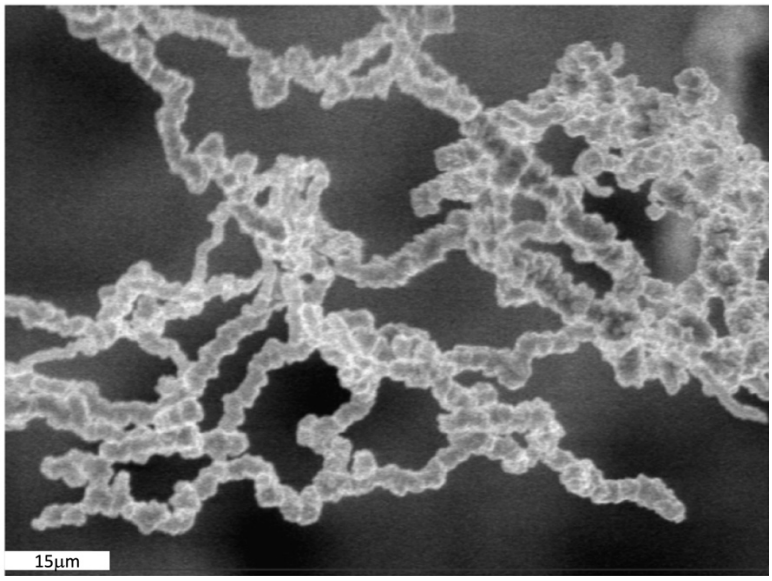

Figure 3-1. Micrograph of nickel nanostrands from Conductive Composites from Johnson [53]. Note that the strands in this image are larger than the average dimensions, but illustrate the typical structure.

The finite element analysis (FEA) focused on the geometrical evolution of two neighboring nanoparticles, and the subsequent modification to the gap between them with strain. The nanoparticles (represented as cylinders) are placed within a block of pure silicone. Outside of the silicone cell is a larger block of homogenous material that combines the properties of the nickel nanoparticles and silicone matrix using the law of mixtures. Boundary conditions were applied to the geometry in the form of constraints to x-direction motion on one face, and application of a specified displacement in the x-direction on the opposite face.

The angle of each nanoparticle was specified with respect to the other nanoparticle and tensile axis using four angles: θ, ϕ, α, β. Figure 3-2 shows a representation of how the axis is affected by the angles and how they affect the positioning of the nanoparticles. In Figure 3-2 the tensile direction is along the x-axis. The angles are applied to the orientation of the system as follows: (1) align both particles with the y-axis, one vertically above the other, with the origin halfway between; (2) rotate both particles about the z-axis in the right-handed sense, by angle θ; (3) rotate the z=z'-axis (and the two particles) about the y'-axis by ϕ in the right-handed sense; (4) rotate the bottom particle by α about the z''-axis in the right-hand sense; (5) rotate the top particle by β about the z''-axis in the right-hand sense. Thus, ϕ and θ affect the axis of the nanoparticles with respect to the tensile axis, and α and β rotate the nanoparticles within the coordinates defined by ϕ and θ.

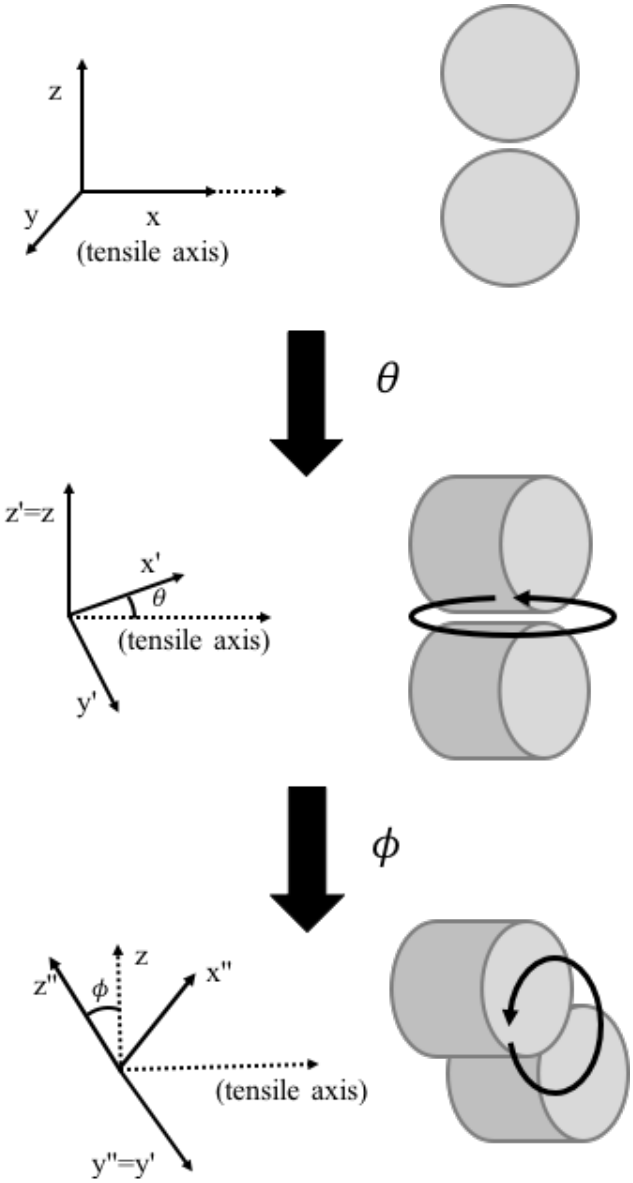

Figure 3-2. Representation of the angles used in FEA. ϕ and θ define the coordinate axes of the fibers with respect to the tensile axes as shown in the figure. The angles α and β are then the rotations of individual nanoparticles about z'' in the right-hand sense.

Initial gap sizes of 2, 3.25, 4.5, and 5.75nm were used for the distance between nanoparticles in the FEA. In an actual sensor, the nanoparticles appear to be pushed together somehow by the manufacturing process or attraction to each other so that the polymer gaps between nanoparticles are very small. Without the nanoparticles being pushed together in some way, the gaps would be much larger. Hence, the thin layer of polymer coating each nanoparticle controls the distance between the particles. The minimum layer of polymer absorbed onto the surface depends on the radius of gyration [54]. Information for the specific polymer used in this study (Ecoflex) were not available, but the range of values reported for PDMS is 1-4nm depending on molecular weight [55]. Other studies assumed a layer of polymer that is one molecule thick would be approximately 1nm [25, 56]. If both nanoparticles had an 1nm thick

adsorbed layer, the total gap would be 2nm. Hence, gaps in this study were assumed to reach a minimum value of around 2nm. This value falls within the range for silicone polymers. Gaps around 2nm also have resistances close to the range of typical conductive materials (about $10^{-4}\Omega m$) according to Equation 1. Gaps up to 5.75nm were chosen to show that even larger initial gaps with resistivities that are in the range of insulative materials (about $10^{6}\Omega m$) can decrease to the conductive range with strain. These five distances were used as bins where any initial gap distance could be assigned and change in gap distance with strain calculated. Any gaps smaller than 2nm were assigned to the 2nm bin and any gaps larger than 5.75nm were assigned to the 5.75nm bin.

From the FEA output of nodal position at each strain interval, the minimum gap distance between neighboring nanostrands could be calculated. The gap distance between the particles is calculated by finding the smallest distance between any node on the first nanoparticle and any node on the second nanoparticle. The data from the FEA was then fit assuming that the smallest possible gap was defined by the thickness of a single polymer molecule (assumed to be approximately 1nm.) The fit of the FEA data also allowed extrapolation of gap size calculation to larger values of strain, beyond those considered by the model. The data from the FEA model covered a range of 0-25% strain. Beyond 25% strain, convergence was sometimes very slow, due to the nonlinear nature of the problem. Furthermore, the resistance model was generally not very sensitive to small errors in gap determination at higher strain values, due to the exponential dependence of resistivity on strain (Equation 1). The typical range of the sensors is between 0-30% for biomechanical applications; hence, the assumed maximum strain for most purposes in this paper is 30%, a relatively small extrapolation beyond the model calculations. The extrapolation also seems reasonable because there are physical limits on the range of the gap even at high values of strain, i.e. the absorbed layer thickness of the polymer being the lower constraint and material flexibility being the upper constraint.

3.1.2 Model Details

Finite element analysis for this work was done in ANSYS 17.2. The simulated nanoparticles were each modeled as cylinders with a radius of 50 nm and length of 1000 nm. As stated earlier, although the physical character of the nanostrands is branched, their high aspect ratio means that any effects of particle curvature are generally at a distance, and the assumption of local linearity should be sufficient. This idea of local linearity also explains why it is reasonable to give all nanoparticles the same length – because the interactions considered in the model are really only a small segment along the length of the two nanostrands. The modeled dimensions were chosen to be within typical values for the radius and aspect ratios. Typical radii range from 25-250nm and aspect ratios of NiNs range from 5-50 [57]. The silicone region had a side length 1200nm and the homogenous material was a block of 3600 nm side length. All sub-

volumes used element type SOLID187. The properties used in the FEA model for each of the materials are listed in

Table 3-1. The density and Poisson's ratio for the homogenous material assumed a volume fraction of 0.54% filler to simulate the behavior of the rest of the sensor.

The mesh for all volumes used tetrahedral elements. The mesh of the nanoparticles divided each cylinder into sections that were about 33 nm in length. The silicone block was divided into elements comprised of 8nm segments and the homogenous block was divided into 10nm segments. These element sizes were chosen after a sensitivity analysis to ensure that the FEA model converged on a consistent prediction of behavior for the system.

Table 3-1. Material properties used in the FEA model.

Material	*Young's Modulus (GPa)*	*Density (kg/m^3)*	*Poisson's Ratio (mm/mm)*
Nickel Nanoparticles	207	8910	0.31
Silicone	1.5e-3	1290	0.45
Homogenous Material	0.57	1330	0.449

3.2 Random Resistor Network

The information from the FEA model was incorporated into a model of a whole nanocomposite sensor by creating a random resistor network (RRN). Each resistor represents a gap between two nanoparticles. The nodes between resistors represent the nanoparticles themselves, but because the resistance of the nickel is so small compared to the resistance of the polymer only the resistance of the gap is considered in the resistor network. Figure 3-3 shows a representation of the resistor network in two dimensions, although a three-dimensional version was actually used. The resistors are attached to a voltage source on one side and to ground on the other.

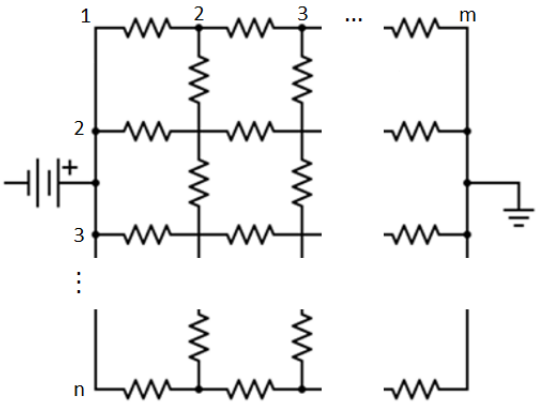

Figure 3-3. Two-dimensional example of a resistor network. The actual random resistor network model used a similar geometry but in three dimensions.

The value of each resistor in the network was found by first assigning initial gap distances (randomly or by some distribution.) The distance then determined the resistance according to Equation 1. As strain was applied to the resistor network, each gap distance changed according to either SPC or FEA. The changed gap distances could then again be converted into resistances. At each value of strain, the overall resistance was calculated using Kirchhoff's current law.

The geometry of the random resistor network in three dimensions is a cubic lattice. The junction gaps in a sensor will not have the same cubic configuration, but it is reasonable to assume that that because of the aspect ratio of the nanoparticles, each is probably connected to at least several other particles just as each node is connected to others in the lattice.

4 RESULTS AND DISCUSSION

4.1 Experimental Verification

The random resistor network (RRN) was validated by comparing the model to resistivity data of an actual nanocomposite sensor. The sensor tested was made of Sylgard 184 with 15% nickel nanoparticles by volume and the resistivity was measured for values of strain between 0 and 60 percent. The dots in Figure 4-1 show the experimental data and the lines show the RRN model using FEA and SPC for gap evolution. The overall shape of the RRN model changes significantly based on the parameters input to the model and the random arrangement of resistances within the network. Even when running the same parameters for nanoparticle angles and initial gap size distribution, the overall shape of the resistivity-strain curve will vary because different resistors end up in different locations. The FEA curve in Figure 4-1 represents a best fit with the smallest square error for the RRN model with FEA when compared with the experimental data. The RRN model with SPC is shown as a comparison using the same parameters including the number of resistors, angles assigned, and initial gap size distribution.

Figure 4-1 used angles for nanoparticle orientation that were randomly distributed along a sphere in the RRN. The distribution for initial gap sizes was a Weibull distribution with a scaling parameter of 3.5nm and a shape parameter of 12.36 (the same value used in Johnson [25]). The mean for the Weibull distribution seems reasonable because it puts initial gap sizes between 1.5nm and 4.2nm. Having one molecule of polymer between two nanoparticles would be 1nm, but there are most likely some gaps that have more than just one molecule between the two nanoparticles. The range of gap sizes with this Weibull distribution seems representative of the polymer gaps in an actual sensor.

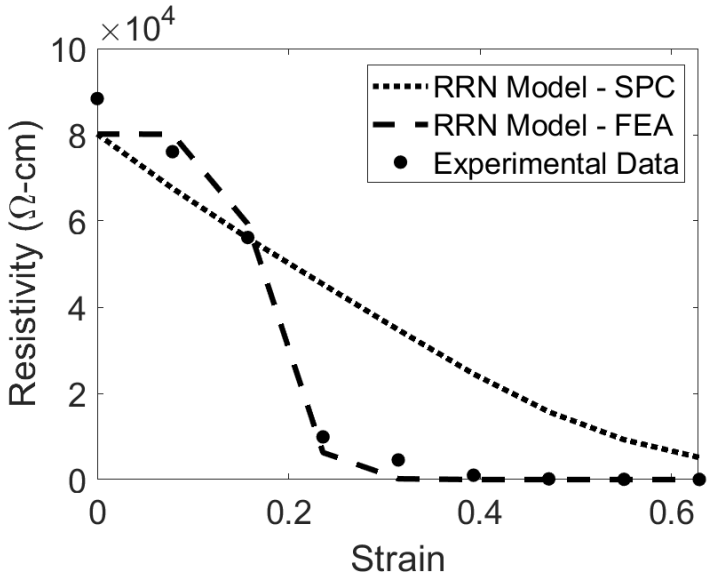

Figure 4-1. Resistivity-strain comparison between experimental data and the random resistor network (RRN) for the best fit. The RRN used angles for nanoparticle orientation randomly distributed along a sphere and a Weibull distribution with a mean of 3.5nm for the initial gap size distribution and a shape parameter of 12.36 (see [25]).

Figure 4-1 compares the performance of the FEA-based gap evolution model with the SPC model for a real sensor. For both models, the alignment and gap distribution was allowed to vary in order to line up with the real data. But only the FEA model was able to find a nanoparticle arrangement that resulted in a close match between predicted and actual resistivity.

4.2 Comparison of Gap Orientation Models (FEA and SPC)

The prediction of gap evolution can have a significant impact on overall resistivity in the RRN. In Figure 4-1, for example, all parameters into the model were kept the same except how gaps evolved with strain but the resulting curves for resistance versus strain of the complete sensor show different behaviors.

In order to compare the Simple Poisson's Contraction model (SPC) with the more detailed FEA approach, various geometrical distributions of filler particles were investigated, and the evolution of the gaps between the particles was predicted by SPC and compared with results from the detailed FEA. The related change in resistance was then modeled for both cases, using the random resistor network model. For the purposes of this discussion, the data from FEA is assumed to be correct and the simplified SPC model is compared with the FEA. The overall resistance of the material was tracked with increased strain, with particular focus on whether resistance was predicted to increase or decrease.

For the initial comparison of the models with differing nanoparticle orientations, the initial gap distribution was a uniform random distribution with values evenly distributed between 3-7nm. The nanoparticles were assigned angles randomly distributed on a sphere for the orientation with respect to the tensile axis (θ and ϕ), and also for the rotation of each nanoparticle (α and β). See Figure 3-2 for a detailed explanation of the angles. In this case, SPC predicted a change in resistance comparable in magnitude and slope to FEA. As seen in Figure 4-2, both gap orientation models predicted that resistance would decrease with strain, matching typical experimental results of the sensors. While there are discrepancies in the actual resistivity values,

the trends are similar. This suggests that SPC may sufficient for modeling the conductive behavior of such materials, if only rough trends are required, when the particles are randomly oriented.

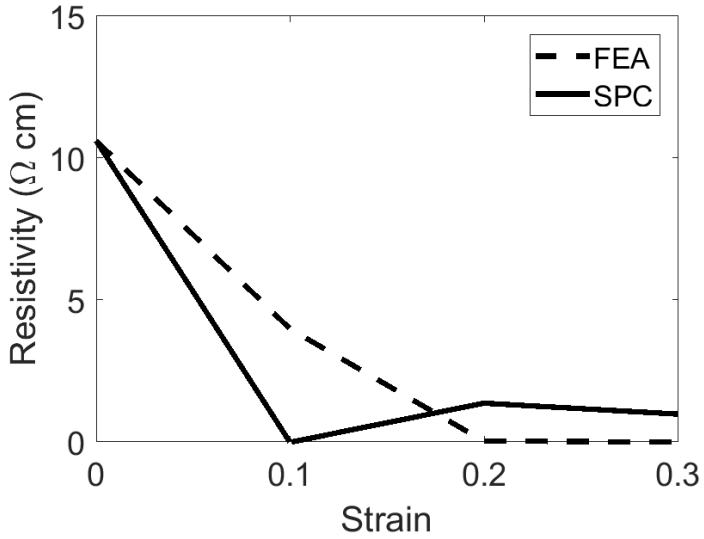

Figure 4-2. Resistivity versus strain for FEA and SPC. The angles for this test were randomly selected on a sphere and the same angles and initial gap sizes were used for both FEA and SPC.

The second example of potential nanoparticle geometry examined the case where particle orientations were restricted to a certain range. Using angles only within a certain range is representative of aligning the nanoparticles within the sensor during the manufacturing process. The rotations of the nanoparticles (α and β in Figure 3-2), which are represented in FEA but not in SPC, appeared to have a significant impact on overall resistivity. One specific case where SPC differed from FEA occurred when all nanoparticles were perpendicular to the tensile direction, i.e. θ equal to 0° and ϕ equal to 90°±15°. SPC predicted that all gaps would increase, causing the overall resistance to increase with strain. In FEA, most of the orientations had gap sizes that increased with strain, however, distributions of orientations where α and β were between 60-90° had gaps that decreased with strain causing the overall resistivity to decrease with strain (see Figure 4-3).

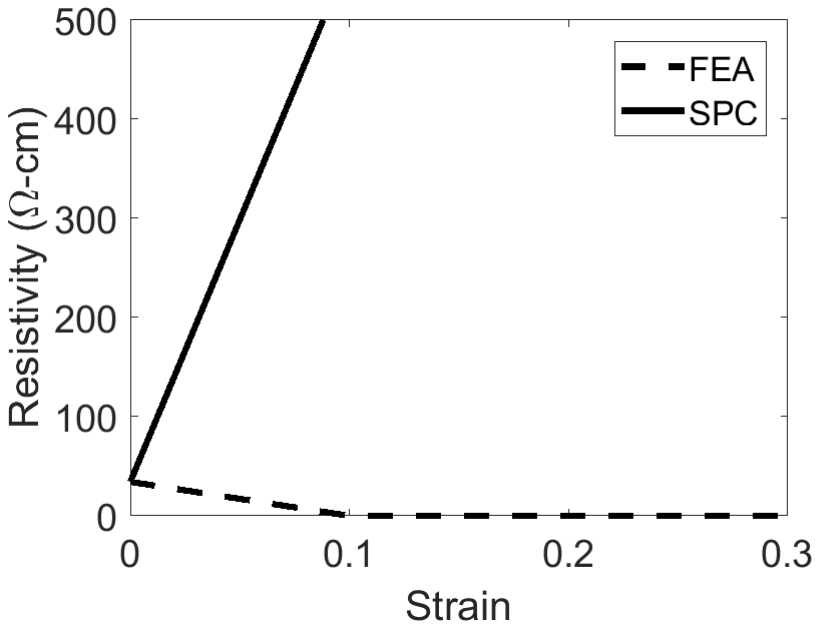

Figure 4-3. Resistance versus strain for FEA and SPC where angles are restricted to within 15° of the tensile axis and α and β in FEA are between 60-90°. SPC predicts a different trend between strain and resistance than FEA in this case but is similar in all other cases.

In order to understand more specifically which orientations of particles behaved differently in the FEA vs the SPC models, the azimuthal (θ) angle (see Figure 3-2) was varied for a particular strain (10% tensile strain), with all gaps set to the same initial value (5nm). Figure 4-4 shows how the distance between nanoparticles (or gap size) changes with strain, for different angles (i.e. particle alignments with the tensile axis). The angles θ and ϕ were combined into a single angle to match the variables defined in the SPC model [25]. The variance in the boxplot for the FEA data comes from the variations of the additional angles defined in the FEA data, i.e. the rotation of each of the nanoparticles or α and β; since the SPC model does not include these additional variables, there is no variance in the predicted result from this model. In each box of the boxplot, the middle line represents the median and the top and bottom lines represent the 75th and 25th percentiles, respectively. Outliers are shown by the red crosses. The difference between FEA and SPC is more pronounced at larger initial gap distances, leading to the selection of the relatively large initial gap size of 5nm for this comparison.

Because of the exponential nature of the tunneling phenomenon (Equation 1), the smaller gaps correlate with large changes in resistance. When gaps are close to 2nm, the resistivity drops dramatically and the gap can conduct electricity. With the SPC model (right), there are no gaps that reach this range after 10% strain; the most significant decrease is a change in gap from 5nm to 4.75nm when the orientation is 90° from the tensile axis. On the other hand, the FEA data (left) predicts that some gaps at every orientation come close to the 2nm (highly conductive) range. Although it is mostly outliers in the boxplot that become conductive, even having a small number of conductive gaps has a large impact on overall resistivity.

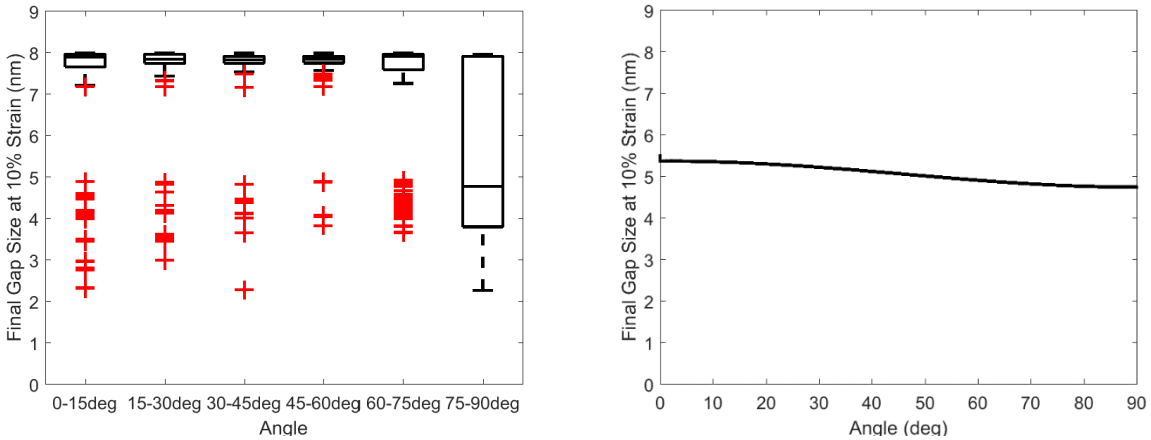

Figure 4-4. Change in gap distance at 10% strain versus angle between nanoparticles. The boxplot (left) shows FEA data and the line (right) shows SPC model.

Figure 4-4 shows that the rotations of nanoparticles (α and β) are important variables to include the full behavior of nanoparticles in order for a model to be accurate. When the particles are randomly oriented, the SPC representation may be incorrect for specific orientations, but the error averages out, resulting in approximately trends of resistivity versus strain (Figure 4-2); but for aligned particles the error is magnified (Figure 4-3).

4.3 Percolation Theory

The percolative behavior of this material with respect to volume fraction of filler has been well-established. As a critical volume fraction (the percolation threshold) of filler is reached, the conductivity increases rapidly as conductive pathways are formed across the sample. One could think about this in terms of an initial empty network spanning the polymer sample. As the volume fraction of filler increases, more connections in the network are 'switched on' by the presence of the filler. Eventually, enough connections are formed that a continuous pathway spans the sample, and conductivity starts to rise significantly.

Similarly, for the strained sample, the hypothetical empty network represents the gaps between the particles. As gaps close under Poisson contraction, the conductivity increases exponentially, according to the quantum tunneling model (Equation 1). It has been hypothesized that this behavior results in a percolation type behavior – i.e. at a certain strain, the number of 'closed' gaps (gaps that are small enough to result in high conductivity or in the range of 2nm or less) reaches a critical fraction and conductive paths form, rapidly increasing conductivity. If the system follows percolation type behavior, there should be the typical s-curve for the conductance increase with strain.

Figure 4-5 shows how conductance is affected by gap size and strain. Gaps were considered 'conductive' with a distance of 2nm or smaller for these figures. Both figures used the random resistor network with angles randomly distributed along a sphere and a uniform random distribution for the initial gap size with values between 2-7nm. The strain was between 0-30%, which is a typical range of use for the conductive polymer sensors. As expected for a percolation-governed system, the conductance increases significantly once the fraction of gaps within the conductive range passes a certain critical value. Although the fraction of conductive gaps does not increase beyond 10 percent, the conductivity in the figure on the left rises from almost zero to nearly 15 Siemens. The figure on the right shows a sharp increase in conductance

as strain increases. It is also important to note that there is a clear s-curve in both plots in Figure 4-5 suggesting that percolation could be an accurate way to model this phenomenon. The figure on the right

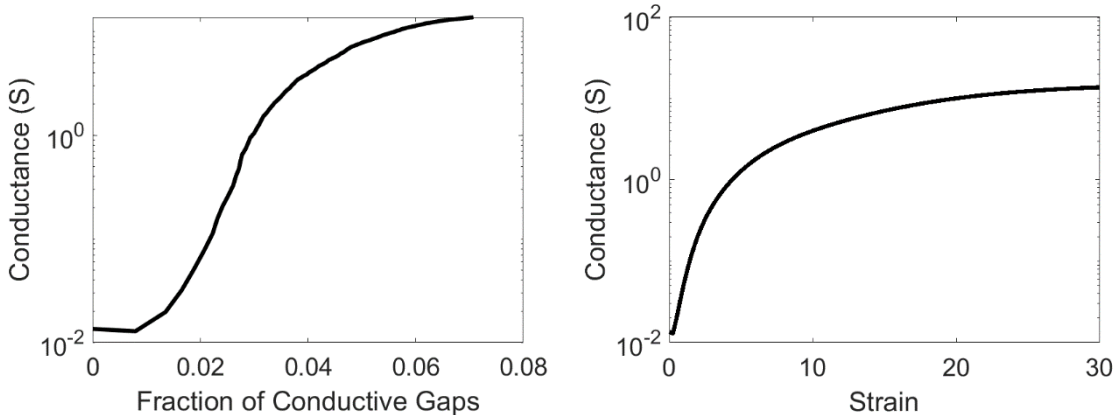

Figure 4-5. Conductance versus the fraction of gaps with a distance less than 2nm (left) and conductance versus strain (right). The conductance increases as more gaps become conductive, as expected. The s-curve is evidence for the ability of percolation theory to accurately model this system.

To further evaluate the viability of percolation models for this system, the RRN was compared to the effective medium (EM) and generalized effective medium (GEM) equations (see Equations 2 and 3) Figure 4-6 shows the random resistor network (RRN) compared to the GEM and EM. The random resistor network in this figure assigned all initial gap distances to a value of 3nm. The values for variables in the GEM/EM equations were taken from Johnson [21] or fit with a least squares approach and are shown in Table 4-1. Table 4-1 also lists a sensitivity analysis showing the percent change in the model response for a ±20% in each input variable. As expected, the variable with the largest change in response is *t*, the exponent for the filler side of the GEM equation. This large change in response is typical for the critical exponents in this equation [47], and given that the conductivity of the filler (nickel) is so much higher than the conductivity of the matrix (silicone), it follows that the exponent for the filler (*t*) would have a larger response than the exponent for the matrix (*s*).

Figure 4-6 shows that the GEM equation fits much more closely to the RRN than the EM equation. This suggests that the piezoresistive effects in the RRN that are not fully captured by simply using the EM equation and confirms that the conductance-strain relationship does follow percolation type behavior.

Table 4-1. Values for the generalized effective medium (GEM) and effective medium (EM) equations used in Figure 4-6. See Equation 3 for GEM and Equation 2 or EM. The model response shows the percent change in the model output for a ±20% in the input parameter.

Variable	*Value*	*Model Response for ±20% Change in Input*	*Source*
σ_m	1.11e-8	±5%	Least Squares Fit

σ_f	2.72e2	±20%	[21]
s	10.37	±10%	[21]
t	1.72	-120% +50%	[21]
ϕ_c	0.0045	±5%	[21]

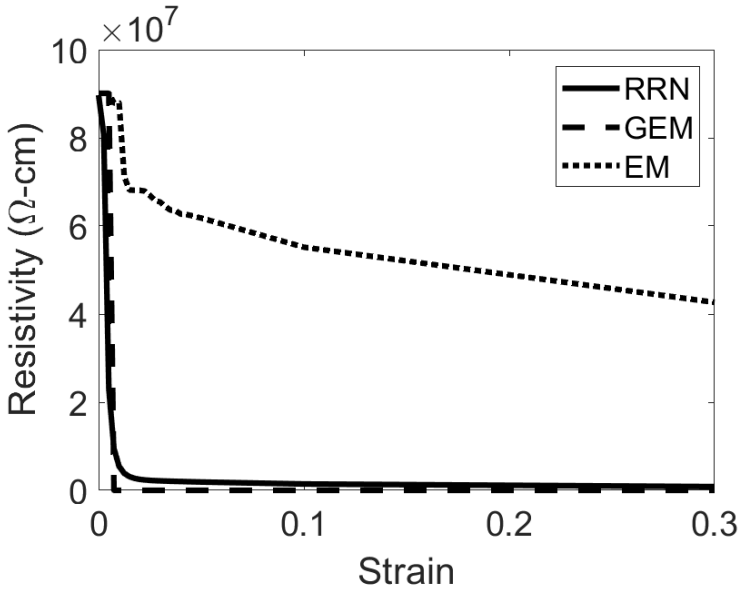

Figure 4-6. Resistivity-strain curves for the random resistor network (RRN) compared to the generalized effective medium (GEM) equation with percolation and the effective medium (EM) equation without percolation theory.

4.4 Design Problem – Gauge Factor

As shown earlier, the orientation of nanoparticles can have a significant impact on resistivity change with strain. From a design perspective, it would be helpful to know, then, what the best orientation of nanoparticles would be to get the greatest gauge factor or change in resistivity for a certain change in strain. The orientations tested were (1) random selection of rotations (defined by θ and ϕ) on the sphere, (2) selecting initial nanoparticle axes (y'' in Figure 3-2) within ±15° of parallel to the tensile axis, (3) selecting initial nanoparticle axes within ±45° from the tensile axis, and (4) selecting initial nanoparticle axes within ±15° of perpendicular to the tensile axis. Within these orientation definitions, varying angles for the rotations of individual nanoparticles (defined by α and β) were also assumed, namely: random rotations, rotations between 0-30°, or rotations between 60-90°.

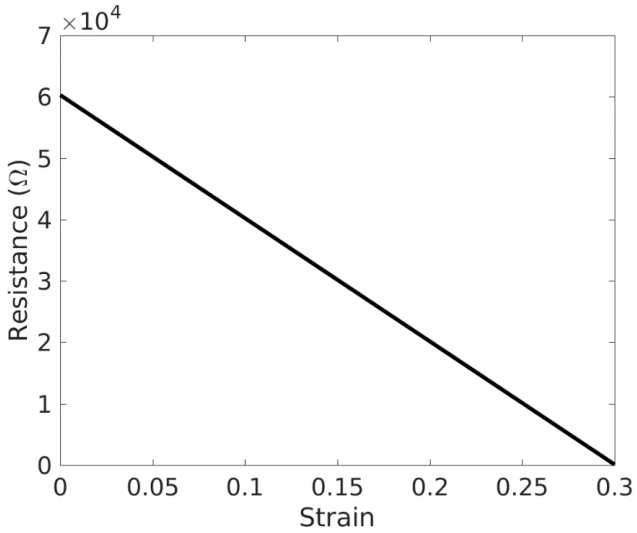

Figure 4-7. Resistivity vs strain for random rotations described by θ and ϕ, but α and β lie between 0-30^o (the particles are aligned relative to each other).

The highest gauge factor, and largest change in resistivity, came from using all possible orientations for the nanoparticle axes (θ and ϕ randomly distributed along a sphere) but restricting the rotations of the nanoparticles to between 0-30° (i.e. by aligning the nanoparticles relative to each other, but not relative to the global frame). Allowing α and β to be any possible values (rather than the range between 0-30°) decreased the gauge factor by 0.5-1. The gauge factor for the example in Figure 4-7 is 3.

4.5 Design Problem – Initial Rise in Resistivity

One phenomenon that happens in the silicone-nickel nanoparticle sensors studied in related work [58] is an initial rise in resistance at small values of strain. The RRN model also usually exhibited the same initial rise in resistance for different resistor networks, though not for all (as seen in earlier figures.) Figure 4-8 shows a curve with the characteristic initial rise in resistivity using the RRN model with FEA. The curve in Figure 4-8 used angles for nanoparticle orientation randomly distributed along a sphere and a Weibull distribution for initial gap sizes with a scaling parameter of 7nm and a shaping parameter of 12.36. The initial spike in resistivity happened with other ranges for the orientation of nanoparticles such as nanoparticles axes within ±45° or ±15°of the tensile axis. The spike happened regardless of the initial gap distribution or mean used, although using a large value for the mean value of initial gap caused the initial rise in resistance to be more pronounced.

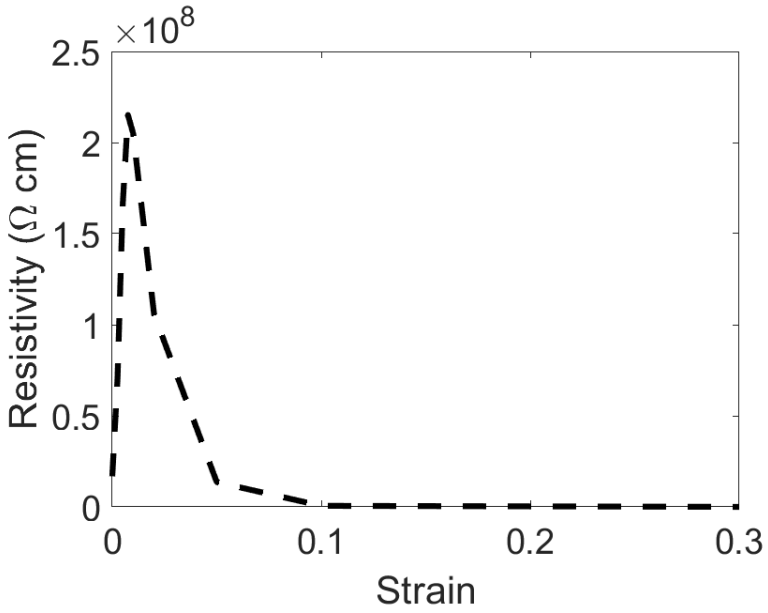

Figure 4-8. A resistivity-strain curve that shows the characteristic initial increase in resistivity seen in experimental data from sensors. This curve used a Weibull distribution with a scaling parameter of 7nm and a shaping parameter of 12.36.

The RRN model with FEA was used to find possible orientations of nanoparticles that remove the initial increase in resistivity. Different ranges of angles between nanoparticles were tested to attempt to find a particular range that would eliminate the initial rise in resistance. When α and β were restricted to be within 0-30°, θ restricted within ±15° of the tensile axis, and ϕ within ±15° of 90° (see Figure 3-2), the initial spike in resistivity disappeared. Figure 4-9 shows an example of one curve with the described restriction in angles.

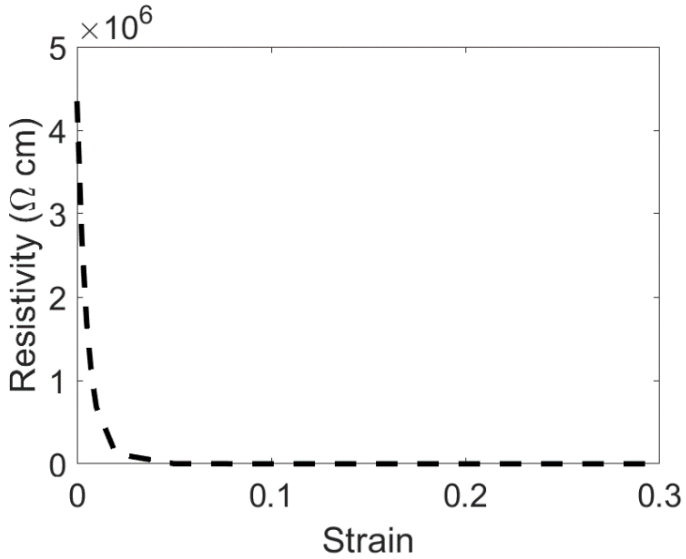

Figure 4-9. Resistivity-strain curve where angles between nanoparticles are restricted to 0-30° for α and β, ±15° of parallel to the tensile axis for θ, and between 75-90° for ϕ. The initial spike in resistance was eliminated when the angles were restricted to the ranges described.

The fact that these angle restrictions eliminated the initial increase in resistivity makes sense since all gaps between nanoparticles at these orientations should decrease with strain according to Poisson's contraction (see Figure 3-2). Hence, it seems that if there were a way to restrict the angles between nanoparticles to a particular range of desired values that it would be possible to remove the unwanted initial spike in resistivity at small values of strain.

5 SUMMARY AND CONCLUSION

The electrical behavior under strain for a nanocomposite sensor was modeled using a random resistor network where the resistance of each polymer gap between two nanoparticles was found using quantum tunneling. This paper analyzed two aspects of the resultant sensor response: (1) How does the nano-particle orientation distribution, as a function of strain, affect the sensor behavior, and can this behavior be adequately captured in a simple Poisson contraction model; and (2) Is the piezoresistivity in the sensor best modeled with percolation theory or is a standard effective medium type approach sufficient?

An FEA model assumed that each nanoparticle was a cylinder (at least, locally) in a silicone matrix. While the cylindrical assumption may not be totally physically accurate, the high aspect ratio of the particles means that any effects from particle curvature are at a distance. There may also be effects from the branched nature of the nanoparticles, but these branching effects would show up in terms of relative alignment of the neighboring nanoparticles. The analytical simple Poisson contraction (SPC) approach assumed that the nanoparticles and matrix could be modeled as a homogenous material, and a Poisson's contraction applied to each gap based upon the gap (rather than the neighboring particles) orientation, in order to predict gap change with global strain. Despite the simpler approach, SPC proved to be effective at capturing the general strain-resistivity behavior for a case where particles were randomly oriented along a sphere. In more specialized cases (e.g. aligning nanoparticles), SPC diverges significant from actual behavior modeled using FEA; for example, SPC predicts that the overall resistivity would increase in various scenarios where FEA shows that it actually decreases. The difference between SPC and FEA stems from the fact that SPC only considers the orientation of the shortest vector between the particles (given by θ and ϕ), without considering the relative orientations of the particles (given by α and β in the FEA simulation). FEA demonstrates that a subset of gaps decreases with strain for a range of θ and ϕ orientations, when the SPC would only predict gap increase for many of these cases. Overall FEA predicts that gaps become 'conductive' (i.e. decrease to around 2nm) from larger initial gap sizes and for a broader number of orientations compared with SPC.

The detailed understanding of how orientation affects gap size available with FEA makes it possible to design a sensor with desired characteristics. The highest gauge factor can be achieved by using all possible orientations for nanoparticles, i.e. angles randomly distributed along a sphere. The initial increase in resistivity seen in real sensors seen in real sensors can be removed by assuming particle geometry where α and β were restricted to be within 0-30°, θ restricted within ±15° of the tensile axis, and ϕ within ±15° of 90°. This range of orientation for the nanoparticles should have all gaps decrease according to Poisson's contraction, so it follows that the overall resistivity would decrease.

Another question answered by this study related to whether the material response of the sensor followed percolation theory. The conductance-strain relationship showed a characteristic s-curve expected in percolative system. There was also an s-curve when plotting conductance

versus the fraction of conductive gaps. Finally, the generalized effective medium equation (GEM) was found to fit the random resistor network much more closely than the effective medium equation. From these findings, it can be concluded that the system does follow a percolation response, and, therefore, modeling the piezoresistivity with percolation theory provides a reasonable estimate of the material response.

ACKNOWLEDGEMENTS

Funding for this research was provided by the National Science Foundation under grant numbers CMMI-1538447.

REFERENCES

1. Kong, J.-H., et al., *Simple and rapid micropatterning of conductive carbon composites and its application to elastic strain sensors.* Carbon, 2014. **77**: p. 199-207.
2. Lu, N., et al., *Highly sensitive skin-mountable strain gauges based entirely on elastomers.* Advanced Functional Materials, 2012. **22**(19): p. 4044-4050.
3. Hassan, G., et al., *Ink-jet printed stretchable strain sensor based on graphene/ZnO composite on micro-random ridged PDMS substrate.* Composites Part A: Applied Science and Manufacturing, 2018. **107**: p. 519-528.
4. Han, J.-E., D. Kim, and K.-S. Yun, *All-polymer hair structure with embedded three-dimensional piezoresistive force sensors.* Sensors and Actuators A: Physical, 2012. **188**: p. 89-94.
5. Firouzeh, A., A.F. Amon-Junior, and J. Paik, *Soft piezoresistive sensor model and characterization with varying design parameters.* Sensors and Actuators A: Physical, 2015. **233**: p. 158-168.
6. Bergström, J. and M. Boyce, *Constitutive modeling of the large strain time-dependent behavior of elastomers.* Journal of the Mechanics and Physics of Solids, 1998. **46**(5): p. 931-954.
7. Boland, C.S., et al., *Sensitive, high-strain, high-rate bodily motion sensors based on graphene–rubber composites.* ACS nano, 2014. **8**(9): p. 8819-8830.
8. Park, J., et al., *Giant tunneling piezoresistance of composite elastomers with interlocked microdome arrays for ultrasensitive and multimodal electronic skins.* ACS nano, 2014. **8**(5): p. 4689-4697.
9. Shin, U.-H., et al., *Highly stretchable conductors and piezocapacitive strain gauges based on simple contact-transfer patterning of carbon nanotube forests.* Carbon, 2014. **80**: p. 396-404.
10. Narongthong, J., et al., *An efficient highly flexible strain sensor: Enhanced electrical conductivity, piezoresistivity and flexibility of a strongly piezoresistive composite based on conductive carbon black and an ionic liquid.* Composites Part A: Applied Science and Manufacturing, 2018. **113**: p. 330-338.
11. Dang, Z.-M., et al., *Supersensitive linear piezoresistive property in carbon nanotubes/ silicone rubber nanocomposites.* Journal of Applied physics, 2008. **104**(2): p. 024114.
12. Sang, Z., K. Ke, and I. Manas-Zloczower, *Effect of Carbon Nanotube Morphology on Properties in Thermoplastic Elastomer Composites for Strain Sensors.* Composites Part A: Applied Science and Manufacturing, 2019.

13. Ferrreira, A., et al., *Electromechanical performance of poly (vinylidene fluoride)/carbon nanotube composites for strain sensor applications.* Sensors and Actuators A: Physical, 2012. **178**: p. 10-16.
14. Wang, X., et al., *Highly sensitive and stretchable piezoresistive strain sensor based on conductive poly (styrene-butadiene-styrene)/few layer graphene composite fiber.* Composites Part A: Applied Science and Manufacturing, 2018. **105**: p. 291-299.
15. Scaffaro, R., et al., *Advanced piezoresistive sensor achieved by amphiphilic nanointerfaces of graphene oxide and biodegradable polymer blends.* Composites Science and Technology, 2018. **156**: p. 166-176.
16. Jiang, X., et al., *Highly Compressible and Sensitive Pressure Sensor under Large Strain Based on 3D Porous Reduced Graphene Oxide Fiber Fabrics in Wide Compression Strains.* ACS applied materials & interfaces, 2019. **11**(40): p. 37051-37059.
17. Gong, S., et al., *Highly Stretchy Black Gold E-Skin Nanopatches as Highly Sensitive Wearable Biomedical Sensors.* Advanced Electronic Materials, 2015. **1**(4).
18. Yao, S. and Y. Zhu, *Wearable multifunctional sensors using printed stretchable conductors made of silver nanowires.* Nanoscale, 2014. **6**(4): p. 2345-2352.
19. Amjadi, M., et al., *Stretchable, Skin-Mountable, and Wearable Strain Sensors and Their Potential Applications: A Review.* Advanced Functional Materials, 2016.
20. Fiorillo, A., C. Critello, and S. Pullano, *Theory, technology and applications of piezoresistive sensors: A review.* Sensors and Actuators A: Physical, 2018. **281**: p. 156-175.
21. Duan, L., D.R. D'hooge, and L. Cardon, *Recent progress on flexible and stretchable piezoresistive strain sensors: from design to application.* Progress in Materials Science, 2019: p. 100617.
22. Amjadi, M., Y.J. Yoon, and I. Park, *Ultra-stretchable and skin-mountable strain sensors using carbon nanotubes–Ecoflex nanocomposites.* Nanotechnology, 2015. **26**(37): p. 375501.
23. Zheng, S., et al., *Highly sensitive and multifunctional piezoresistive sensor based on polyaniline foam for wearable Human-Activity monitoring.* Composites Part A: Applied Science and Manufacturing, 2019. **121**: p. 510-516.
24. Canavese, G., et al., *Piezoresistive flexible composite for robotic tactile applications.* Sensors and Actuators A: Physical, 2014. **208**: p. 1-9.
25. Johnson, O.K., et al., *Multiscale model for the extreme piezoresistivity in silicone/nickel nanostrand nanocomposites.* Metallurgical and Materials Transactions A, 2011. **42**(13): p. 3898-3906.
26. Koecher, M., et al., *Characterization of nickel nanostrand nanocomposites through dielectric spectroscopy and nanoindentation.* Polymer Engineering & Science, 2013. **53**(12): p. 2666-2673.
27. Kalantari, M., et al., *A new approach for modeling piezoresistive force sensors based on semiconductive polymer composites.* IEEE/ASME Transactions on Mechatronics, 2012. **17**(3): p. 572-581.
28. Luheng, W., D. Tianhuai, and W. Peng, *Influence of carbon black concentration on piezoresistivity for carbon-black-filled silicone rubber composite.* Carbon, 2009. **47**(14): p. 3151-3157.

29. Paredes-Madrid, L., et al., *Underlying Physics of Conductive Polymer Composites and Force Sensing Resistors (FSRs) under Static Loading Conditions.* Sensors, 2017. **17**(9): p. 2108.
30. Zhang, X.W., et al., *Time dependence of piezoresistance for the conductor-filled polymer composites.* Journal of Polymer Science part B: polymer physics, 2000. **38**(21): p. 2739-2749.
31. Hu, N., et al., *Tunneling effect in a polymer/carbon nanotube nanocomposite strain sensor.* Acta Materialia, 2008. **56**(13): p. 2929-2936.
32. Oskouyi, A.B., U. Sundararaj, and P. Mertiny, *Tunneling conductivity and piezoresistivity of composites containing randomly dispersed conductive nano-platelets.* Materials, 2014. **7**(4): p. 2501-2521.
33. Simmons, J.G., *Generalized formula for the electric tunnel effect between similar electrodes separated by a thin insulating film.* Journal of applied physics, 1963. **34**(6): p. 1793-1803.
34. Bilodeau, R.A., et al., *Evolution of nano-junctions in piezoresistive nanostrand composites.* Composites Part B: Engineering, 2015. **72**: p. 45-52.
35. Meier, J.G., J.W. Mani, and M. Klüppel, *Analysis of carbon black networking in elastomers by dielectric spectroscopy.* Physical Review B, 2007. **75**(5): p. 054202.
36. Hansen, N., D.O. Adams, and D.T. Fullwood, *Quantitative methods for correlating dispersion and electrical conductivity in conductor–polymer nanostrand composites.* Composites Part A: Applied Science and Manufacturing, 2012. **43**(11): p. 1939-1946.
37. Zhou, Y., et al., *A novel route towards tunable piezoresistive behavior in conductive polymer composites: addition of insulating filler with different size and surface characteristics.* Composites Part A: Applied Science and Manufacturing, 2017. **96**: p. 99-109.
38. McLachlan, D., et al., *The correct modelling of the second order terms of the complex AC conductivity results for continuum percolation media, using a single phenomenological equation.* Physica B: Condensed Matter, 2003. **338**(1): p. 256-260.
39. McLachlan, D.S., M. Blaszkiewicz, and R.E. Newnham, *Electrical resistivity of composites.* Journal of the American Ceramic Society, 1990. **73**(8): p. 2187-2203.
40. Alig, I., et al., *Dynamic percolation of carbon nanotube agglomerates in a polymer matrix: comparison of different model approaches.* physica status solidi (b), 2008. **245**(10): p. 2264-2267.
41. Lei, H., et al., *Modeling carbon black/polymer composite sensors.* Sensors and Actuators B: Chemical, 2007. **125**(2): p. 396-407.
42. Lysenkov, E. and V. Klepko, *Analysis of Percolation Behavior of Electrical Conductivity of the Systems Based on Polyethers and Carbon Nanotubes.* Journal of Nano-and Electronic Physics, 2016. **8**(1): p. 1017-1.
43. Yi, X.S., G. Wu, and Y. Pan, *Properties and applications of filled conductive polymer composites.* Polymer international, 1997. **44**(2): p. 117-124.
44. Deng, H., et al., *Effect of melting and crystallization on the conductive network in conductive polymer composites.* Polymer, 2009. **50**(15): p. 3747-3754.
45. Barton, R., J. Keith, and J. King, *Development and modeling of electrically conductive carbon filled liquid crystal polymer composites for fuel cell bipolar plate applications.* Journal of New Materials for Electrochemical Systems, 2007. **10**(4): p. 225.

46. Hussain, M., Y.-H. Choa, and K. Niihara, *Fabrication process and electrical behavior of novel pressure-sensitive composites.* Composites Part A: applied science and manufacturing, 2001. **32**(12): p. 1689-1696.
47. Zhou, J., et al., *Percolation transition and hydrostatic piezoresistance for carbon black filled poly (methylvinylsilioxane) vulcanizates.* Carbon, 2008. **46**(4): p. 679-691.
48. Xu, S., et al., *The viability and limitations of percolation theory in modeling the electrical behavior of carbon nanotube–polymer composites.* Nanotechnology, 2013. **24**(15): p. 155706.
49. Balberg, I., *Tunneling and nonuniversal conductivity in composite materials.* Physical Review Letters, 1987. **59**(12): p. 1305.
50. Rakowski, W.A. and M. Kot, *Thermal stress model for polymer sensors.* Journal of Thermal Stresses, 2004. **28**(1): p. 17-28.
51. Taya, M., W. Kim, and K. Ono, *Piezoresistivity of a short fiber/elastomer matrix composite.* Mechanics of materials, 1998. **28**(1): p. 53-59.
52. Kale, S., et al., *Effect of filler alignment on percolation in polymer nanocomposites using tunneling-percolation model.* Journal of Applied Physics, 2016. **120**(4): p. 045105.
53. Johnson, O.K., et al., *The colossal piezoresistive effect in nickel nanostrand polymer composites and a quantum tunneling model.* CMC: Computers, Materials, & Continua, 2010. **15**(2): p. 87-112.
54. Chen, B. and J.R. Evans, *Nominal and effective volume fractions in polymer− clay nanocomposites.* Macromolecules, 2006. **39**(5): p. 1790-1796.
55. Higgins, J., K. Dodgson, and J. Semlyen, *Studies of cyclic and linear poly (dimethyl siloxanes): 3. Neutron scattering measurements of the dimensions of ring and chain polymers.* Polymer, 1979. **20**(5): p. 553-558.
56. Litvinov, V. and P. Steeman, *EPDM− Carbon Black interactions and the reinforcement mechanisms, as studied by low-resolution 1H NMR.* Macromolecules, 1999. **32**(25): p. 8476-8490.
57. Johnson, O.K., et al., *Deciphering the structure of nano-nickel composites*. 2009, Los Alamos National Laboratory (LANL): SAMPE 2009.
58. Baradoy, D.A., *Composition Based Modaling of Silicone Nano-Composite Strain Gauges.* 2015.